Probing the electronic structure in $M_2Mo_6Se_6$: Quadrupole couplings measured by NMR

Benjamin G. M. Chew, Josh H. Golden, Beth A. Huggins, Francis J. DiSalvo, and David B. Zax*
Baker Laboratory, Department of Chemistry, Cornell University, Ithaca, New York 14853
(Received 25 January 1994; revised manuscript received 11 May 1994)

Nuclear-magnetic-resonance spectroscopy has been used to probe the electronic structure of the M cationic sites in $M_2Mo_6Se_6$, M =(Li,Rb,Cs,In), a family of low-dimensional electronic conductors. Measured values of the quadrupole coupling parameter constant are compared to calculated values of the contribution from an ionic lattice. The measured values deviate significantly from calculation only for M=In, where the observed value substantially exceeds the calculated value. This deviation is attributed to an In p-orbital contribution to the conduction band. Such a contribution would provide a mechanism for the interchain electronic coupling observed in $M_2Mo_6Se_6$ chain systems when M=In or Tl.

I. INTRODUCTION

Potel and co-workers[1] have described a series of pseudo-one-dimensional $M_2Mo_6Se_6$ compounds where M is a monovalent cation chosen from among the group IA or group IIIA metals. Structurally, the compounds consist of stacked Mo_3Se_3 triangles displaced by 60° from one another extending infinitely along the crystalline hexagonal c axis. The chains are separated by the monovalent cations. Depending on the size of M, a typical chain-chain distance is approximately 9 Å (Fig. 1), measured center to center.

Electronic properties of isolated $(Mo_3Se_3)_n^{n-}$ chains have been calculated based on an extended Hückel model.[2] At room temperature the valence electron donated from each M is delocalized along the Mo_3Se_3 unit along the crystalline c axis, and the chains are conductors. At low temperatures, however, a Peierls distortion is suggested which would localize these electrons and the ground state is semiconducting (as it must be for a truly one-dimensional system). Of course, the calculations admit the metal ions only as electron donors and explicitly ignore their possible contribution, and that of nearby chains, to the electronic structure, and hence cannot be expected to predict possible coupling between chains.

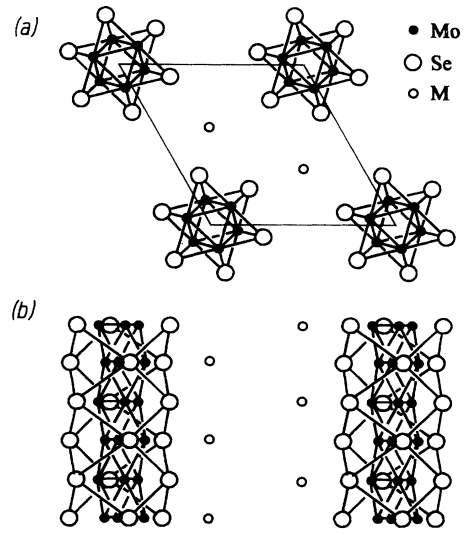

FIG. 1. Structure of $M_2Mo_6Se_6$. (a) Projection onto the (001) plane. (b) Projection onto the $(11\bar{2}0)$ plane.

Resistivity measurements of Tarascon *et al.*[3] have shown that where M is an alkali metal a transition from metallic to semiconducting behavior is found at low temperature, which is consistent with predictions based on the one-dimensional band-structure calculations.[2] Where M is In or Tl, however, no semiconducting transition is observed; in fact, $Tl_2Mo_6Se_6$ undergoes a superconducting transition at 5.1 K. These observations are inconsistent with electrons localized in one dimension, and suggest the importance of a detailed consideration of the role of the cations in the electronic structure of the $M_2Mo_6Se_6$ lattices. Our goal in this paper is to explore the electronic structure of the cations between the conducting chains. Our primary tool will be solid state nuclear magnetic resonance (NMR).

Our procedure in this paper is as follows. First, we describe our samples. The theoretical basis for understanding the electric field gradient is then presented. We continue by presenting our approach to measuring these gradients. The correlation between measured gradients and lattice and electronic structure is then made. We close by mentioning some related experiments using magic angle spinning (MAS) which further clarify our conclusions.

II. EXPERIMENTAL

A. Sample preparation

Samples were prepared as described in detail in earlier work by Tarascon *et al.*[4] $In_2Mo_6Se_6$ was initially prepared from the elements at 1000 °C. The alkali metal

phases are subsequently prepared by ion exchange, where the $In_2Mo_6Se_6$ is mixed with alkali iodide and heated to approximately 500 °C. Indium iodide sublimes away, and the alkali metal cation substitutes for the lattice In^+. The progress of the reaction can be monitored by x-ray powder diffraction and scanning electron microprobe analysis until the indium-based phase is no longer observed.

Each of the $M_2Mo_6Se_6$ phases crystallizes in a hexagonal unit cell belonging to space group $P6_3/m$. The c-axis dimension varies little from phase to phase, as it is primarily determined by the bonding in the $Mo_6Se_6{}^{2-}$ repeat unit. In contrast, the chain-to-chain spacing (which is reflected in the a lattice parameter) varies nearly linearly with alkali metal ionic radius, except where M=Li.[4] In $Li_2Mo_6Se_6$, it appears that the lithium cations are so small that electrostatic repulsion between pairs of chains dominates the interchain spacing.

Even after the InI is removed, we have frequently found that sample crystallinity of the lithium samples (as measured by NMR linewidths) can be improved by subsequent annealing at relatively low (~200 °C) temperatures for several hours.

B. Electric field gradients

The dominant nuclear spin interaction (excluding that of the nuclear dipole moment with the applied magnetic field) for most nuclei where $I \geq 1$ is that of the spin nuclear quadrupole moment with any local electric field gradient (EFG). Local field gradients can be an exquisitely sensitive probe of local structure, providing a marker sensitive to the extent of local order/disorder. For example, in NaCl the symmetry of the perfect cubic lattice allows for no electric field gradient, and any splitting or broadening necessarily reflects defects and lattice imperfections.

This work, however, focuses instead on a different property of the EFG—its ability to reveal local electronic structure. Cohen and Reif[5] have provided a framework for this approach. More recently, Taylor, Baugher, and Kriz,[6] Kaufmann and Vianden,[7] and Carter, Bennett, and Kahan[8] have provided comprehensive reviews of the subject, and we present a quick summary of these results here.

In a perfect crystal, the net field gradient at the nucleus is composed of two separable contributions, one associated with the field arising from a distribution of charged ions (q_i) and a second associated with the local distribution of valence electrons (q_v). In cases of high symmetry (e.g., a cubic lattice, or all electrons found in closed spherically symmetric shells) either contribution may vanish, but in general the observed gradient is given by

$$eq_{\text{total}} = (1 - R_s)eq_v + (1 - \gamma_\infty)eq_i. \tag{1}$$

The parameters γ_∞ and R_s are the Sternheimer factors[9] which account for the polarization of the closed-shell electrons as they interact with local field gradients. The closed-shell electrons may either screen or amplify the effect of external gradients on the nucleus buried within. Different screening factors are appropriate depending upon whether the field gradient is associated with internal (R_s) or external (γ_∞) sources.

Magnetic resonance measurements provide an experimental measure of $e^2q_{\text{total}}Q/h$, where eQ is the nuclear quadrupole moment and measures the asymmetry of the charge distribution in the nucleus. Thus our experiments should provide a direct probe of the magnitude of eq_{total}. Our goal in this paper is to analyze the extent to which these measurements of local EFG's at the various metal sites can be interpreted in terms of differences in electronic structure in the metal molybdenum selenides.

Even in similar lattices with similar eq's, $e^2q_{\text{total}}Q/h$ at different cations may range over four or five orders of magnitude due to variations in eQ and γ_∞. As a result, no single technique of extracting the quadrupole couplings is universally applicable. In this work, three spectroscopic methods have been exploited for the extraction and/or estimation of quadrupolar parameters in our samples. Energy splittings in these systems depend upon not only e^2qQ/h but also the spin quantum number I, and the spectroscopic splittings may be more appropriately characterized by a parameter $\nu_Q = 3e^2qQ/2I(2I-1)h$.

Depending upon the relative sizes of ν_Q, the rf excitation strength ν_{rf}, and the size of other sources of broadening, differing experiments may be appropriate. For very large quadrupole coupling constants, it may be easiest to measure their size via techniques associated with pure nuclear quadrupole resonance, or NQR, where the only strongly allowed transitions appear at frequencies

$$\nu_m = \tfrac{1}{2}\nu_Q(1 - 2m), \tag{2}$$

where m is the spin moment of the initial state. The spectrum consists of a series of equally spaced lines associated with transitions originating from the various possible initial states signified by m. Traditional NQR methods are most appropriate where the transition frequencies appear at sufficiently high frequencies (preferably above 10 MHz) that sensitivity is good. This is rarely the case for the alkali metals.

For relatively small values of ν_Q, quadrupole-perturbed NMR experiments are most common. In the presence of a large applied field, first-order perturbation theory leads us to modify Eq. (2) so that the quadrupolar interaction is observed as an additional splitting of magnitude

$$\nu_m^{(1)} = \tfrac{1}{4}\nu_Q(1 - 2m)(3\cos^2\theta - 1), \tag{3}$$

centered at the nuclear Larmor frequency, where m is the expectation value of I_z (referenced, now, to the z axis defined by the applied field) in the initial state, and θ is the angle between the locally defined axis system of the field gradient and the macroscopically defined axis system defined by the applied field. Again, for any given orientation this corresponds to a series of equally spaced lines, and if θ is known, knowledge of $\nu_m^{(1)}$ is equivalent to knowledge of ν_Q. Figure 2(a) shows a calculated single crystal spectrum for an $I = 5/2$ nucleus with $\nu_Q = 9$ kHz and $\theta = 90°$.

In polycrystalline samples, the distribution of orientations yields a spectrum consisting of a distribution of fre-

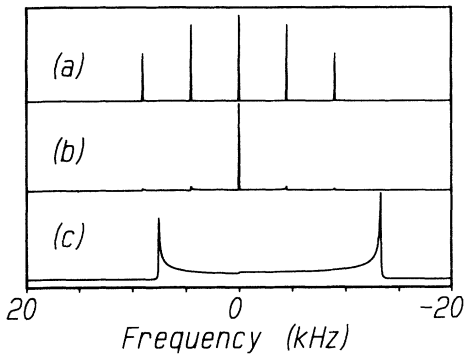

FIG. 2. Simulations of axially symmetric quadrupolar powder patterns, as a function of ν_Q. Each simulation assumes a Larmor frequency of 100 MHz. (a) Single crystal spectrum of an $I = 5/2$ nucleus with $\nu_Q = 9$ kHz and $\theta = 90°$. Lines correspond to the $|5/2\rangle \rightarrow |3/2\rangle$, $|3/2\rangle \rightarrow |1/2\rangle$, $|1/2\rangle \rightarrow |-1/2\rangle$, $|-1/2\rangle \rightarrow |-3/2\rangle$, and $|-3/2\rangle \rightarrow |-5/2\rangle$ transitions. (b) Powder spectrum of an $I = 5/2$ nucleus with $\nu_Q = 9$ kHz. Note that the sharp singularities correspond to the $\theta = 90°$ position of the EFG as seen in (a). (c) Powder spectrum of the central transition ($|1/2\rangle \rightarrow |-1/2\rangle$) of an $I = 3/2$ nucleus with $\nu_Q = 2100$ kHz.

quencies, intensity weighted according to the probability of finding a particular orientation. For example, $\theta = 0°$, where the EFG tensor is aligned along the applied field, is less likely than $\theta = 90°$, where the EFG tensor is aligned perpendicular to the applied field. Figure 2b shows the calculated typical powder pattern intensity distributions associated with randomly oriented field gradient tensors for an $I = 5/2$ system with $\nu_Q = 9$ kHz. Each of the individual transitions $|m\rangle \rightarrow |m-1\rangle$ is associated with a powder pattern distribution including a singularity in the intensity distribution corresponding to the $\theta = 90°$ orientation. If the singularities are clearly observed, simultaneous knowledge of their frequency and orientation again makes it possible to extract ν_Q.

As ν_Q increases, the powder pattern increases in breadth proportionately, unless $m = 1/2$, since $\nu_{1/2}^{(1)} = 0$. As NMR probes and receivers are narrow banded, often the singularities associated with the outer transitions are unobserved. In such cases there may be no directly accessible experimental probe of ν_Q.

Under conditions where only the central transition can be observed, an indirect technique can still provide an estimate of ν_Q. The quadrupole nutation experiment requires that we vary the applied rf field used to excite magnetization. Where the applied rf field ν_{rf} is large compared to ν_Q, the signal intensity after a pulse of length τ_p (observed in the central transition only) is proportional to $\sin \nu_{rf}\tau_p$. Where ν_{rf} is small compared to ν_Q, the observed signal intensity is proportional to $\sin(I+1/2)\nu_{rf}\tau_p$. Where ν_{rf} and ν_Q are comparable, the signal intensity is a complex function of the ratio of the two. Calculated nutation spectra as a function of ν_Q/ν_{rf} and I have been published by Samoson and Lippmaa[10] and by Kentgens *et al.*,[11] and a comparison between the observed and calculated spectra provides a reasonable estimate of ν_Q even where only the central transition is observed. The accuracy of these measurements, at least in our hands, appears limited (by rf inhomogeneity, the finite step size associated with the simulations, or our neglect in the analysis of large chemical shift anisotropies).

For sufficiently large quadrupole couplings ($\nu_Q \sim 500$ kHz), the central transition becomes structured and shows well-defined singularities. This can be explained by second-order perturbation theory. For axially symmetric field gradients the orientation-dependent second-order quadrupolar shift from the Larmor frequency ν_L for the central transition is

$$\nu_{1/2}^{(2)} = \frac{\nu_Q^2}{16\nu_L}[I(I+1) - \tfrac{3}{4}](\cos^2\theta - 1)(9\cos^2\theta - 1). \quad (4)$$

Figure 2(c) shows a calculated second-order quadrupole-perturbed powder pattern corresponding to the central transition of an $I = 3/2$ nucleus with $\nu_Q = 2.1$ MHz and axial symmetry. The frequency separation Δ of the two sharp singularities is

$$\Delta = \frac{25\nu_Q^2}{144\nu_L}[I(I+1) - \tfrac{3}{4}], \quad (5)$$

and ν_Q is readily derived once Δ is measured.

All three of these methods have been used to obtain the quadrupolar coupling constants for the cation sites of the various samples. The experimentally determined ν_Q's are presented below.

C. Isotropic shifts

The average resonance frequency deviates from the Larmor frequency by a small amount

$$\nu_{obs} = \gamma B_0(1 - \delta_{obs}), \quad (6)$$

where γ is the gyromagnetic ratio, B_0 is the magnetic field strength, and δ_{obs} is the observed isotropic shift of the nucleus. There are three contributions to the total observed isotropic shift,

$$\delta_{obs} = \delta_{iso}^{(CS)} + \delta_{iso}^{(KS)} + \delta_{iso}^{(2Q)}, \quad (7)$$

where the first term is the isotropic chemical shift, the second is the isotropic Knight shift, and the last is the isotropic second-order quadrupolar shift. The chemical shift is due to the localized electronic distribution. The presence of conducting electrons gives rise to a Knight shift.[12] In addition to broadening the features of the central transition, second-order quadrupole effects also shift the center of mass of the entire pattern. The isotropic second-order quadrupolar shift is given (in ppm) by[13,14]

$$\delta_{iso}^{(2Q)} = -\frac{1}{30}\left(\frac{\nu_Q}{\nu_L}\right)^2[I(I+1) - 3/4] \times 10^6. \quad (8)$$

The isotropic shift can be used to characterize the electronic environment surrounding the nucleus.

D. Measured quadrupolar couplings

All experiments were performed on a home-built spectrometer, based on a 7.05 T wide-bore magnet, operating at Larmor frequencies of 39.3640 MHz for ^{133}Cs, 65.7029 MHz for ^{115}In, 98.1800 MHz for ^{87}Rb, and 116.5920 MHz for ^{7}Li. Variable temperature studies were performed in a CF1200 continuous flow cryostat from Oxford Instruments and home-built probes. Where magic angle spinning was required, commercial probes capable of spinning 7 mm rotors (Doty Scientific, Inc.) and 7.5 mm rotors (Chemagnetics) were used.

In this work we have studied $M_2Mo_6Se_6$ systems for M=Li, Rb, Cs, and In. For each of the alkali metals, the highest abundance naturally occurring nuclear isotopes have quadrupole moments. For several of them, there are multiple quadrupolar nuclear spin species—e.g., ^{6}Li ($I = 1$) and ^{7}Li ($I = 3/2$), or ^{85}Rb ($I = 5/2$) and ^{87}Rb ($I = 3/2$). Spectra of any of the available isotopes should similarly reflect the electronic field gradient at that site. In this work we will focus, therefore, on only our results from the single nuclear spin species where the Larmor frequency was highest and the signal was easiest to observe—i.e., ^{7}Li, ^{87}Rb, and ^{115}In for the multiple-isotope nuclei and ^{133}Cs for the nucleus with only a single spin-active isotope. There are additional NMR-active nuclei associated with K (but of unfortunately low frequency) and Tl (but as both isotopes have $I = 1/2$ there is no quadrupole moment and therefore neither is sensitive to electric field gradients).

As the lattice structures are similar independent of cation, we assumed that the field gradients eq_i would differ relatively little from sample to sample. Most of the variability in ν_Q for the alkali metals (where the electron contribution eq_v should vanish) was expected to derive from the differing magnitudes of eQ and γ_∞. As such we expected ν_Q to increase in the progression Li→Cs→Rb.

With its small quadrupole moment, we expected to easily observe the full spectrum (central transition and singularities associated with the $|3/2\rangle \rightarrow |1/2\rangle$ and $|-1/2\rangle \rightarrow |-3/2\rangle$ transitions) for the lithium sites in $Li_2Mo_6Se_6$. It was somewhat of a disappointment when the spectrum of $Li_2Mo_6Se_6$ when first received [Fig. 3(a)] showed a rather featureless line shape with no apparent structure. As no change was observed upon cooling [Fig. 4(a)], it was concluded that there was no dynamic disorder and little evidence of Li^+ mobility at room temperature. However, upon heating to 480 K we observed substantial spectral narrowing, indicating fast motion of the Li^+ cations [Fig. 4(c)]. When cooled slowly back to room temperature (ca. 1°/min), the structured spectrum of Fig. 3(b) was observed. In the low-temperature annealed sample, the singularities expected to indicate the quadrupole-perturbed transitions are clearly shown,

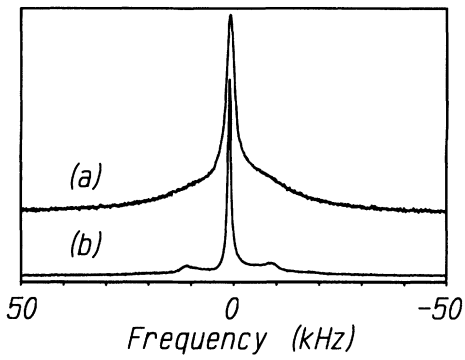

FIG. 3. ^{7}Li ($I = 3/2$) spectrum of $Li_2Mo_6Se_6$ at room temperature. $\nu_L = 116.592$ MHz. (a) As received. (b) After heating at 480 K for approximately 3 h. The singularities of the outer transitions are clearly shown. From the position of the $\theta = 90°$ portion of the $|3/2\rangle \rightarrow |1/2\rangle$ transition, $\nu_Q = 19.6$ kHz.

and the powder pattern is readily analyzed and suggests $\nu_Q \approx 19.5$ kHz.

Room temperature spectra of the ^{133}Cs in $Cs_2Mo_6Se_6$ showed some suggestion of the singularities expected to correspond to the outer transitions in this multilevel system ($I = 7/2$). However, we could not unequivocally correlate between a singularity and a specific nuclear spin transition, as the spectrum was substantially broadened with respect to the ideal quadrupolar powder pattern, and there also appeared to be a substantial chemical shift anisotropy. Nutation spectra were observed as a function of the applied rf field strength for relatively weak fields (typically 3–15 kHz). One concern was that the rf field was sufficiently weak that other interactions (e.g., chemical shift anisotropies and/or dipolar couplings) might be of comparable size. A second concern was that an analy-

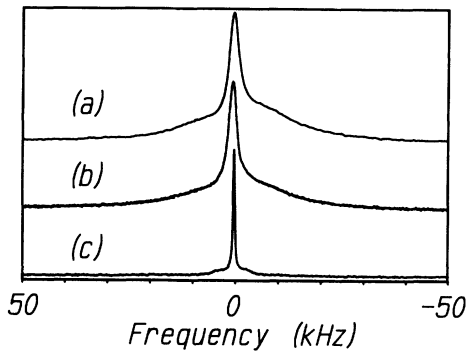

FIG. 4. ^{7}Li ($I = 3/2$) spectrum of $Li_2Mo_6Se_6$. $\nu_L = 116.592$ MHz. (a) 77 K. No change in the linewidth from (b) 298 K. (c) 480 K shows substantial narrowing of the spectrum, indicating fast motion of the lithium cations.

sis of the nutation experiment proceeds from the expectation that only the central transition is observed. It was not obvious that this condition holds in our experiment. Under these conditions, a series of six experiments with varying rf strengths ν_{rf} yielded measured values of ν_Q of 28 ± 2 kHz.

The relatively large values of eQ and γ_∞ for Rb led us to expect much larger quadrupolar interactions. This was confirmed by our observation of a structured central transition spectrum from the ^{87}Rb nuclei in $Rb_2Mo_6Se_6$ at room temperature [Fig. 5(a)]. The clearly defined singularities located at the edges of the second-order powder pattern are characteristic of an axially symmetric quadrupolar coupling, and the width is given by Eq. (5) above. We find an experimental value of $\nu_Q = 3624$ kHz.

The room temperature ^{115}In spectrum of $In_2Mo_6Se_6$ in Fig. 6 is most reminiscent of the analogous ^{87}Rb spectrum. Again we see a central transition line shape characteristic of an axially symmetric quadrupolar coupling tensor. Based on our analysis of the second-order pattern's width we measured $\nu_Q = 1310$ kHz. So as to confirm this observation, we subsequently performed a series of experiments where the exciting rf irradiation pulse was swept to lower and higher frequencies, with the hope that we might observe some of the low-intensity first-order quadrupolar-split transitions associated with this $I = 9/2$ nucleus.

The full spectrum is shown in Fig. 7. The figure corresponds to 30 separate experiments, displayed simultaneously on the same spectrum. The exciting rf frequency was incremented between experiments by 200 kHz steps. At each stage the probe was retuned and the pulse widths adjusted to account for the differing excitation efficiencies associated with each quadrupolar transition,[15] although it is difficult to be certain that intensities are reliable across the entire spectrum. Nonetheless, it was gratifying to observe so clearly the signal intensity peaks corresponding to the $\theta = 90°$ portion of the powder pattern

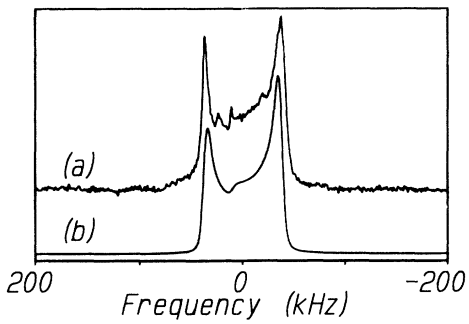

FIG. 5. (a) ^{87}Rb ($I = 3/2$) spectrum of $Rb_2Mo_6Se_6$ (room temperature), central transition ($|1/2\rangle \rightarrow |-1/2\rangle$), showing a second-order quadrupolar splitting. The splitting between the two sharp singularities gives a ν_Q of 3624 kHz. The line shape indicates that the EFG is axially symmetric ($\eta = 0$). $\nu_L = 98.18$ MHz. (b) Simulated spectrum using the calculated value of $\nu_Q = 3618$ kHz.

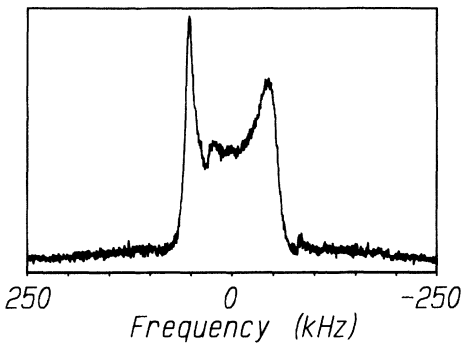

FIG. 6. ^{115}In ($I = 9/2$) spectrum of $In_2Mo_6Se_6$ (room temperature), central transition ($|1/2\rangle \rightarrow |-1/2\rangle$), showing a second-order quadrupolar splitting. $\nu_L = 65.7029$ MHz. From the splitting between the two sharp singularities, ν_Q is measured to be 1310 kHz. The line shape also indicates that the EFG is axially symmetric ($\eta = 0$).

[associated with the transitions (c) $|-3/2\rangle \rightarrow |-5/2\rangle$, ($d$) $|-1/2\rangle \rightarrow |-3/2\rangle$, ($e$) $|1/2\rangle \rightarrow |-1/2\rangle$, ($f$) $|3/2\rangle \rightarrow |1/2\rangle$, and ($g$) $|5/2\rangle \rightarrow |3/2\rangle$] at precisely the frequencies predicted by our analysis of the second-order powder pattern. The unobserved singularities (associated with transitions (a) $|-7/2\rangle \rightarrow |-9/2\rangle$, ($b$) $|-5/2\rangle \rightarrow |-7/2\rangle$, ($h$) $|7/2\rangle \rightarrow |5/2\rangle$, and ($i$) $|9/2\rangle \rightarrow |7/2\rangle$] are spread over 5 MHz, and we saw little reason to pursue them further.

In the case of the ^{115}In, where we have analyzed a second-order spectrum, the pattern is noticeably dis-

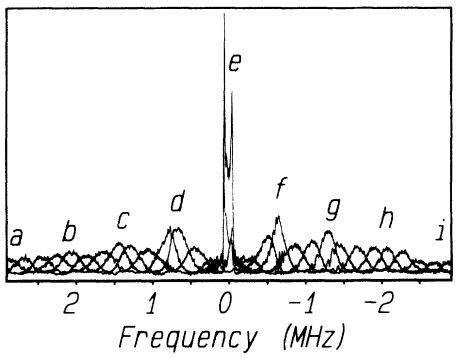

FIG. 7. Full ^{115}In ($I = 9/2$) spectrum of $In_2Mo_6Se_6$ (room temperature). 30 individual spectra were taken with the excitation frequency incremented in 200 kHz steps and the pulse widths accordingly adjusted as discussed in the text. The center of the spectrum corresponds to $\nu_L = 65.7029$ MHz. The singularities of the (c) $|-3/2\rangle \rightarrow |-5/2\rangle$, ($d$) $|-1/2\rangle \rightarrow |-3/2\rangle$, ($e$) $|1/2\rangle \rightarrow |-1/2\rangle$, ($f$) $|3/2\rangle \rightarrow |1/2\rangle$, and ($g$) $|5/2\rangle \rightarrow |3/2\rangle$) transitions are clearly observed. The outer transitions, (a) $|-7/2\rangle \rightarrow |-9/2\rangle$, ($b$) $|-5/2\rangle \rightarrow |-7/2\rangle$, ($h$) $|7/2\rangle \rightarrow |5/2\rangle$, and ($i$) $|9/2\rangle \rightarrow |7/2\rangle$) are spread over 5 MHz, and are difficult to discern.

torted from that of the ideal second-order pattern. In particular, the up-field (low frequency) singularity is of lower intensity (and perhaps more broadened). It has been suggested[16] that this reflects some lattice disorder; it may also be an artifact of the particular excitation sequences used to obtain the time-domain spectra. The observation of first-order satellites consistent with the analysis of the second-order pattern ignoring this distortion leads us to believe that no fundamental features are ignored in the process.

E. Predicting the lattice contribution eq_i

1. *Lattice summation: background*

Given the lattice constants and symmetries derived from x-ray diffraction data, it should be a simple matter to calculate the ionic contribution to local field gradients. The $\alpha\beta$th component (for $\alpha, \beta = x,\ y,$ or z) of the field gradient tensor V due to a distribution of surrounding charges is[17]

$$V_{\alpha\beta} = \int \frac{\rho}{4\pi\epsilon_0}\left(\frac{3\alpha\beta - \delta_{\alpha\beta}r^2}{r^5}\right)d\tau \qquad (9)$$

for the charge density ρ of the distribution and $\vec{r} = (x, y, z)$ the internuclear vector. Each of the tensor elements may be generated from this expression. In our problem, each cation occupies a site of threefold symmetry with respect to rotations about the crystalline c axis. This high lattice symmetry guarantees that the field gradient is identical along any axis in the a-b plane, i.e., is axially symmetric. Laplace's equation ($\nabla^2 V = 0$, or the field gradients in the three canonical directions sum to 0) and this axial symmetry ensure that only one parameter—V_{zz}—is sufficient to describe completely the lattice contribution to the field gradient tensor (where the field gradient z axis coincides with the crystalline c axis), and Eq. (9) reduces, for the V_{zz}th component, to

$$V_{zz} = \int \frac{\rho}{4\pi\epsilon_0}\left(\frac{3\cos^2\theta - 1}{r^3}\right)d\tau. \qquad (10)$$

Despite the apparent simplicity of Eq. (10), attempts to calculate lattice contributions to nuclear quadrupole couplings are relatively infrequent. Early efforts have suggested that the convergence of the implied lattice summation was poor.[7] The argument against convergence of the sum goes roughly as follows. The contribution of a particular ionic site to the field gradient at some other site in the lattice varies with $1/r^3$, where r is the internuclear distance. As any sum over all lattice points must necessarily sum over spheres of increasing radius, and (on average) the number of lattice points increases as r^2, the contribution from successive radial shells varies as $1/r$. But it is well known that infinite sums over $1/r$ do not converge.

The fallacy in this argument is clear. Ions must "perform" the very same calculation we have described above in order to know what field gradient they experience. As quadrupole couplings in well-ordered crystals are finite and measurable, the associated field gradients must be similarly finite in size and, therefore, the sum must be convergent. Our problem, then, is to discover a procedure which emphasizes the convergent aspects of the problem so as to efficiently calculate quadrupole coupling constants.

A basic outline of the solution follows; a more detailed description is provided below. A simple prescription for calculating field gradients seems to require attention to the following details.

(1) The second derivative of the potential V_{zz} varies as $P_2(\cos\theta)$, i.e., the field gradient tensor is highly directional. Positive contributions from the angular dependence are found in cones with angle 54.74° above and below any given point charge, whereas negative contributions are found everywhere else. Any numerical summation which works by calculating sets of lattice points in $\{x, y, z\}$ coordinate space is likely to cover all of the positive contributions quite readily; but in any x-y plane, many of the negative contributions are at long distances. A simple solution is available—as $P_2(\cos\theta)$ vanishes when integrated over a sphere, an opportune basis set for any numerical integration is to operate in shells of increasing r integrating in $\{r, \theta, \phi\}$ space.

(2) The lattice sum should exploit the symmetry of the lattice—i.e., the lattice summation should be considered not over lattice points, but over unit cells in the lattice. At sufficiently large distance, the electric field due to charges located in an electrically neutral cell must fall off more rapidly with distance than does a dipolar field. Problems of convergence appear to be often associated with summations which sum over all ions within a specified sphere, rather than over complete cells which fall within that sphere. This may appear to be a fine distinction; nonetheless, a simple argument suggests the difference. At the surface of the sphere, where partial cells which need not be electrically neutral are included, the field due to these isolated charges does not necessarily converge.

2. *A multipole expansion*

Our model for the lattice summation is as follows. We take for the lattice constants the extensive x-ray compilations of Tarascon *et al.*[4] which describe a lattice belonging to space group $P6_3/m$. Each cation is assumed to be singly ionized and its electron donated to the molybdenum selenide chains. We further assume that the electron density is uniform along the conducting chains so that V_{cc}, the field gradient along the crystalline c axis, is 0. Under these conditions and for our lattice symmetry, there is no contribution to the field gradient at the cation lattice sites from electrons in the conducting chains. Thus the lattice sum over the charge distribution ρ in Eqs. (9) and (10) can be restricted to a summation

over the cation distribution.

Simmons and Slichter[18] provide a procedure for running the calculation using a multipole expansion to sum over electrically neutral Wigner-Seitz cells. Their multipole expansion gives the potential V_{zz} for a lattice of point charges as a discrete sum,

$$V_{zz} = \sum_i \sum_R \frac{q}{4\pi\epsilon_0} \sum_{n=0}^{\infty} \frac{1}{n!} \left[\frac{\partial^2}{\partial z_i^2} \left(\vec{R} \cdot \vec{\nabla}_i \right)^n \right] \frac{1}{|\vec{r}_i + \vec{R}|_{r_i}}, \tag{11}$$

where $\vec{r}_i = (x_i, y_i, z_i)$ is the vector from the origin to the center of the Wigner-Seitz cell, $\vec{R} = (x, y, z)$ is the vector from the center of the cell to the lattice points, and $\vec{\nabla}_i = (\frac{\partial}{\partial x_i}, \frac{\partial}{\partial y_i}, \frac{\partial}{\partial z_i})$. The monopole ($n$= 0) and dipole ($n$= 1) terms of the expansion vanish due to the neutrality and the symmetry of the cell, and so the first term of the expansion is the quadrupole term (n= 2). These terms have an (R^{n-2}/r_i^n) dependence. Since R is limited by the size of the Wigner-Seitz cell, the terms converge quite rapidly with the distance r_i.

The multipole expansion only holds for large r_i. Therefore a direct lattice sum is performed on the cations within the first 25 Å radius, being careful to include only complete cells. The multipole expansion is then used on the cations in the annulus from 25 Å to the final radius of the summation.

Calculations were performed on a SPARCStation IPC from SUN Microsystems. Table I shows the contribution of the expansion terms up to $n = 6$ for $Rb_2Mo_6Se_6$. The direct lattice sum over the first 25 Å yields $V_{zz} = eq_i = 1.020\,244 \times 10^{14}$ Hz/e Å^2. The quadrupole term ($n = 2$) changes the calculated field gradient by 0.12%. The higher-order corrections fall off quite rapidly. Table II compares the direct lattice sum and the multipole expansion as the radius of the summation sphere increases. The difference at 25 Å is due to the inclusion of partial cells at the surface of the sphere in the direct lattice sum. Clearly, the multipole expansion converges much more quickly than does the direct lattice sum. As seen in Table II, increasing the summation radius from 75 Å to 100 Å only changed the value of eq_i in the seventh significant digit, while the calculation time on the workstation doubled. The smallness of the multipole corrections suggests that the straightforward sum over the lattice is reasonably adequate, and similar conclusions have been recently reached by others[19–22] as well. However, the multipole expansion was still used out to 100 Å and $n = 6$ for our samples.

TABLE I. Multipole expansion calculation in a sphere of radius 100 Å for $Rb_2Mo_6Se_6$. A direct lattice sum is taken over the first 25 Å, being careful to include complete Wigner-Seitz cells. The multipole expansion is performed in the annulus between 25 Å and 100 Å.

	eq_i (10^{14} Hz/e Å^2)	Change (%)
25 Å direct sum	1.020 244	
$n = 2$	1.021 474	+0.1205
$n = 3$	1.020 862	−0.0599
$n = 4$	1.020 411	−0.0442
$n = 5$	1.020 135	−0.0270
$n = 6$	1.020 006	−0.0126

TABLE II. Calculated eq_i. Comparison of direct lattice sum and multipole expansion ($n = 6$) for $Rb_2Mo_6Se_6$.

Radius of summation (Å)	eq_i Direct sum (10^{14} Hz/e Å^2)	eq_i Multipole expansion (10^{14} Hz/e Å^2)
25	1.012 619	1.020 244
50	1.015 336	1.019 984
75	1.023 083	1.020 007
100	1.027 883	1.020 006

Table III gives the calculated values for the field gradients as a function of cation. In accordance with our expectation, the ionic contribution eq_i (based on our assumption of complete ionization) varies only modestly as a function of cation. Most of the positive contributions to the field gradient are associated with positively charged ions above and below the origin of our problem, which depend on the lattice parameter c and which vary little with cation size. Most of the negative contributions to the field gradient are associated with positively charged ions displaced along the a or b lattice directions, and are smaller for larger unit cells (larger cations).

F. The spectroscopic splittings

Calculation of spectroscopic splittings requires a knowledge of both the nuclear quadrupole moments (eQ) and the scaling factor $(1 - \gamma_\infty)$. The former are generally measured to a reasonably high degree of accuracy. However, there appears to be some disparity in the literature values of the quadrupole moment of ^{133}Cs. The quadrupole moment is very small, and so the accuracy of the measurement is inherently smaller than for larger moments. The reported value of Q for ^{133}Cs varies from −0.002 b to −0.004 b.[23–25]

The atomic polarizabilities represented by γ_∞ are generally known only theoretically and are available in standard references[26] as well as scattered throughout the literature. For the ionized alkali metals, the Sternheimer factors are available. No comparable theoretical value for In^+ exists. Therefore, we must proceed with a best estimate.

Mohapatra[27] has recently reported γ_∞ for In (neutral) as −21.7, and further suggests that the polarizability should decrease in magnitude as electrons are removed. In that spirit, his calculations show $\gamma_\infty \approx -12.40$ for Zn and $\gamma_\infty \approx -11.54$ for Zn^{2+}. Furthermore, all calculations suggest that in isoelectronic systems the magnitude of Sternheimer factors decreases rapidly with increasing nuclear charge when the numbers of protons and electrons are comparable, and so γ_∞ for In^+ is almost certainly smaller in magnitude than for the isoelectronic species Cd ($\gamma_\infty \approx -30.85$). We will subsequently assume

TABLE III. Calculated $\nu_Q = 3e^2q_{calc}Q(1-\gamma_\infty)/2I(2I-1)h$ vs measured $\nu_Q = 3e^2qQ/2I(2I-1)h$ for various $M_2Mo_6Se_6$'s.

M	γ_∞	Q (10^{-8} Å^2)	eq_{calc} (10^{13} Hz/e Å^2)	$\lvert\nu_Q\rvert_{calc}$ (kHz)	$\lvert\nu_Q\rvert_{expt}$ (kHz)
$^7Li^+$	0.255	−0.0366	9.294 863	12.7	19.6
$^{133}Cs^+$	−110.81	−0.002 to −0.004	11.878 87	18–36	28±2
$^{87}Rb^+$	−52.781	0.132	10.200 06	3618	3624
$^{115}In^+$	∼ −20	0.861	9.915 574	750	1310

$\gamma_\infty \leq -21.7$ for In^+, and a value of approximately −20 appears reasonable. Small errors in determining γ_∞ will have little impact on our ultimate conclusions.

III. DISCUSSION

A. Comparison of experimental and theoretical values

Based on the calculated values of eq_i and the available values of eQ and γ_∞ taken from literature sources, we arrived at the theoretical values of the spectroscopic splitting provided in Table III. We first focus on the three alkali metals. For ^7Li in $Li_2Mo_6Se_6$, where the Sternheimer factors are small, the calculated value of ν_Q is significantly smaller than is observed. This is somewhat puzzling. For a well-ordered lattice, most of the possible discrepancies would lead to overestimates of ν_Q, not underestimates. In particular, if the Li site is only partially ionized then the calculated quadrupolar coupling constant eq_i should be scaled by the percentage of ionization. Were there residual electronic charge remaining on the cation, the only available orbitals in Li are spherically symmetric and do not contribute to eq_v.

For ^{133}Cs in $Cs_2Mo_6Se_6$, it is somewhat difficult to compare the experimentally observed value with the calculated value. Our confidence in the spectroscopic measurements is limited (as explained above). Furthermore, it appears that for Cs eQ is known with only limited accuracy as discussed above. Therefore we do not find small discrepancies significant, and the measured value is within the range given by the accuracy of eQ.

For ^{87}Rb in $Rb_2Mo_6Se_6$, we have, perhaps fortuitously, an excellent match between calculated and observed values of ν_Q, where the two values differ by less than 1.0%. This is particularly important, as the technique of measurement—based on an analysis of the width of the second-order quadrupolar powder pattern—is identical to that used in the analysis of the In spectrum in $In_2Mo_6Se_6$. A simulated spectrum based on the calculated value of ν_Q is shown in Fig. 5. The close agreement between calculation and experiment suggests that, at least for Rb, our lattice model for the ionic contribution to the field gradient is reasonable and provides a full explanation for the observed spectroscopic splittings.

The In and Rb species have values of ν_Q of comparable magnitude, and both are measured by an analysis of the second-order quadrupole splitting of the central transition. Nonetheless, our calculated value for eq_i in the In-based compound (which is essentially the same for the two cations of similar size) substantially underestimates the observed spectroscopic splitting for any reasonable values of the Sternheimer factors. Given that similar spectroscopic techniques were used, this deviation of almost a factor of 2 between calculation and measurement for In is certainly significant.

B. Explaining the deviations

As noted above, the significant deviations between theory and experiment are found for the cases of ^7Li in $Li_2Mo_6Se_6$ and ^{115}In in $In_2Mo_6Se_6$. This was particularly puzzling for the former, since the only accessible electronic states in Li are the $1s$ and $2s$ orbitals. As each has spherical symmetry, neither should contribute to the field gradient eq_v and so the entire contribution to ν_Q should be attributable to eq_i.

A separate NMR probe is available for the investigation of local electronic environments. The isotropic resonance frequency (ignoring some small second-order shifts associated with large quadrupolar couplings) varies with local chemical and/or electronic environment. In solids, where the largest interactions are anisotropic, special techniques are required to measure the isotropic shift with high precision. The most common method involves spinning the sample about an axis tilted 54.74° with respect to the main field (the so-called "magic angle"). At slow spinning rates, the spectrum breaks up into a peak at the isotropic chemical shift flanked by sidebands at multiples of the spin rate. The magic angle spinning (MAS) spectrum of ^7Li shows two distinct Li environments in $Li_2Mo_6Se_6$ at room temperature [Fig. 8(a)]. Varying the spin rate and identifying the spin-rate-independent lines provides a simple method of identifying the isotropic peak(s). In our spectrum we find two overlapping patterns of Li shifts and sidebands, with isotropic shifts 1.9 ppm and −1.0 ppm referenced to $1M$ aqueous LiCl. In contrast, the ^{133}Cs MAS spectrum [Fig. 8(b)] indicates only one distinct site.

NMR studies of lithium intercalated in molybdenum cluster chalcogenides have been recently presented by Prigge *et al.*[28] They have studied a series of compounds of chemical formula $Li_xMo_6Se_8$, for $1 \leq x \leq 4$. These compounds are related to our systems as endcapped monomers of our polymeric repeating unit. These authors find a dramatic variation in the isotropic value of the Li shift as x changes. These shifts can be classified as primarily due to chemical effects (i.e., as chemical

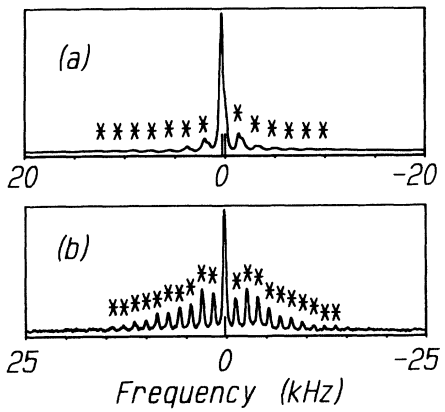

FIG. 8. Spinning about the "magic angle" (54.74° with respect to the main field) breaks up the powder pattern into a peak at the isotropic chemical shift and sidebands (denoted by *'s) at multiples of the spin rate, revealing finer chemical details. (a) ^{7}Li MAS spectrum of $Li_2Mo_6Se_6$. ν_L = 116.592 MHz. This clearly shows the existence of two Li sites. The isotropic shifts are 1.9 ppm and −1.0 ppm referenced to 1M aqueous LiCl. Spin rate is 1.7 kHz. (b) ^{133}Cs MAS spectrum of $Cs_2Mo_6Se_6$. ν_L = 39.364 MHz. In contrast to the ^{7}Li spectrum in (a), there is only one distinct site in this compound. The isotropic shift is at 400 ppm from 0.5M aqueous CsCl. Spin rate is 5.5 kHz.

shifts due to localized electronic distributions) or electronic effects (i.e., as Knight shifts due to conduction electrons) by measuring T_1 relaxation rates at various temperatures. A Knight shift is indicated when the Korringa relationship[12] holds, $T_1 \propto 1/K^2T$, where K is the Knight shift and T is temperature.

Prigge *et al.*[28] further report isotropic shifts as large as 111 ppm for $Li_3Mo_6Se_8$, and as small as 3 ppm for $Li_4Mo_6Se_8$ (referenced to aqueous LiCl). Based on T_1 relaxation data, these authors have identified the large shifts as Knight shifts, and the small shifts as ionized Li^+ cations. Our shifts are similarly small, and the temperature dependence of our Li T_1 measurements is inconsistent with a substantial Knight shift contribution to the relaxation. This demonstrates that there is negligible overlap of the Li s orbitals with the conduction band in $Li_2Mo_6Se_6$.

Furthermore, we observe what appear to be two distinct isotropic shifts, indicating at least two distinct Li sites with slightly different chemical environments. This is, of course, inconsistent with the x-ray lattice classification which suggests only a single cation site, but this is not surprising due to the small size of the Li^+ cation. Because the Li^+ cation cannot be directly seen by x ray, its position has been determined by the locations of the surrounding atoms. It has previously been observed[4] that the lattice constant a shrinks in proportion to the cation radius, except for when Li^+ replaces Na^+. As electrostatic repulsive forces work to maintain a distance of minimum approach between chains, the small Li^+ cation appears not to occupy a single, well-defined lattice site. Due to the low electron density at the Li^+ cation, this deviation from the symmetry of the ideal $P6_3/m$ space group may be unobservable using x rays. It is, however, consistent with a quadrupole coupling constant different from that calculated on the assumption of the atomic coordinates of $P6_3/m$ symmetry.

In the alkali-metal-based molybdenum selenides, we believe our simple model for the field gradient is therefore predictive. However, there remains a large deviation in the indium molybdenum selenide. This deviation is particularly surprising in that the lattice parameters and spectroscopic measurement techniques are most similar to those employed in the analysis of the $Rb_2Mo_6Se_6$, where our predictions most closely reproduced the observed value of ν_Q. There is, however, one particular difference between the two cases.

In the alkali metals, there are no low-lying electronic orbitals which can contribute to eq_v. This is not necessarily the case in $In_2Mo_6Se_6$, where the In cation releases an electron to the chains from its singly occupied p orbital. In an atomic beam experiment, Kusch and Eck[29] measured the quadrupole splitting for In containing one p electron. They found $(1-R_s)e^2q_vQ/h = -899$ MHz. Based on Eq. (1) above, which represents the total eq at the nucleus, we can calculate a partial occupancy for the In p orbital. An axially symmetric total field gradient is possible only if eq_i and eq_v have the same principal axes. As our calculations predict eq_i is axially symmetric with respect to the crystalline c axis, the partially occupied p orbital must be axially symmetric with respect to that same axis. Moreover, eq_i and eq_v are of opposite sign to one another. While we do not know experimentally the absolute sign of the spectroscopically determined quadrupole coupling, we do know that its magnitude exceeds that of eq_i; therefore it must be negative, like eq_v. Thus, with $(1-\gamma_\infty)e^2q_iQ/h = 18$ MHz, and $e^2q_{\text{total}}Q/h = -31$ MHz, we have

$$p \text{ occupancy} = \frac{|e^2q_{\text{total}}Q/h| + |(1-\gamma_\infty)e^2q_iQ/h|}{|(1-R_s)e^2q_vQ/h|} \approx 0.05.$$

Note that this partial occupancy is sufficiently small that rescaling the ionic contribution to reflect the average positive charge of only 0.95 would change the above conclusions only minimally. This partial occupancy is also consistent with electronegativity arguments which predict that the indium would be less likely than the alkali metals to donate its valence electron.

C. Isotropic shifts

A partially ionized orbital may lead to a Knight shift. We may measure the isotropic indium shift [referenced to a saturated aqueous solution of $In_2(SO_4)_3$] from the singularities in the central transition, and $\delta_{\text{obs}} = -347$ ppm. Calculating the second-order quadrupolar contribution

to this shift from Eq. (8), one obtains $\delta_{iso}^{2Q}=-288$ ppm, leaving approximately -59 ppm for either a chemical shift or a Knight shift. Pure indium metal has been observed to have a Knight shift of 0.82% at 300 K.[8] Since indium metal donates three electrons to the conduction band and the $In_2Mo_6Se_6$ donates one electron from each indium atom, we must also scale the 5% p-orbital occupancy by a factor of one-third. This indicates that we should look for a Knight shift at 300 K of 140 ppm, which should be large enough to see easily. However, because indium chemical shifts can range from 440 ppm to -555 ppm,[30] it would be difficult to distinguish between a chemical shift and a Knight shift in this case.

The measured isotropic shift in the rubidium compound is $\delta_{obs} = 185$ ppm from $1M$ aqueous $RbNO_3$. δ_{iso}^{2Q} is calculated to be -136 ppm. The Knight shift in pure rubidium metal is 0.6693% at 300 K and 0.6643% at 4 K.[8] Again assuming a partial occupancy of the s orbital in the $Rb_2Mo_6Se_6$ of 5%, we should be looking for a Knight shift on the order of about 330 ppm. The isotropic chemical shift range for rubidium varies from 183 ppm for RbI to -53 ppm for Rb_2CrO_4.[31] The $Rb_2Mo_6Se_6$ sample was cooled to 6 K. No substantial change in either the size of the quadrupole coupling or in the isotropic shift was observed between 300 K and 6 K. In addition, Korringa-like behavior of the T_1's was not observed over this temperature range, which would indicate that the Knight shift has a small contribution to the total observed shift. However, the alkali metal molybdenum selenides have the additional complication of the conductivity changing at low temperatures. A change in the resistance of $Rb_2Mo_6Se_6$ has been reported[3] at about 60 K. Again, it would be difficult to definitely assign a Knight shift or chemical shift in this case.

The ^{133}Cs MAS spectrum [Fig. 8(b)] indicates a single site, which is supported by the x-ray powder diffraction data, with an isotropic shift of 400 ppm from $0.5M$ aqueous CsCl. Using the Korringa relationship and the T_1T relationship for cesium metal,[8] if this were a Knight shift, the T_1 at room temperature should be about 0.5 sec. The T_1 at room temperature of this compound is about 45 sec, which is inconsistent with a Knight shift. This shift also appears to be sample dependent. We have observed a 400 ppm range of isotropic shifts for different samples of $Cs_2Mo_6Se_6$. However, the different samples all have approximately the same size quadrupole coupling constants (within 10%). Since these shifts do not appear to be due to Knight shifts, they do not impact on our conclusions.

Isotropic ^{77}Se shifts ($I = 1/2$) have been measured by MAS on these compounds. While we observe differences in the isotropic shifts over a 50 ppm range, the full range of ^{77}Se shifts covers about 1500 ppm.[31] In addition, the band-structure calculations[2] indicate negligible electron density at the selenium sites. Because of this, we do not expect the electronic structure of the chains to have an impact on our results.

IV. CONCLUSION

A number of studies have demonstrated that there is a substantial difference between the electronic structure in alkali molybdenum selenides and group IIIA molybdenum selenides. This difference is manifested in bulk properties such as the low-temperature transition to a semiconducting phase found in the former compounds, and a superconducting phase in some of the latter compounds. These bulk properties are indicative of microscopic differences in the electronic structure and are characteristic of one-dimensional structures (in the alkali molybdenum selenides) or multidimensional structures (in the indium or thallium molybdenum selenides). The mechanism by which chains might couple has not previously been determined.

In this work we have used as our probe of local electronic structure the interaction of nuclear quadrupole moments with electric field gradients. Quantitative comparisons of theoretical and experimental values are relatively rare, apparently due to the perceived difficulty in performing the necessary lattice sums. We believe those difficulties are overestimated, and that, with modern computers and well-chosen summation strategies, good results are readily achievable. In our case, we find that calculations and experiments yield the same quadrupole coupling constant for Rb in $Rb_2Mo_6Se_6$. For Li in $Li_2Mo_6Se_6$, we find that a low-temperature annealing process at 200 °C transforms a disordered lattice into a better-ordered array, presumably by Li^+ diffusion. The lattice thereby produced is not that observed in the x-ray structures (which are relatively insensitive to Li positions) in that at least two Li environments are observed. Under these conditions, the quadrupole coupling constant is not expected to be calculable as we no longer have the appropriate coordinates to enter into the lattice summation.

The magnitude of the quadrupolar coupling constant measured for In in $In_2Mo_6Se_6$ cannot be explained in the same fashion as for Rb, despite the similarities in lattice parameters and methods of measurement. By invoking a valence electron contribution to the measured quadrupole coupling we can account for the observed field gradient by assuming partial conduction band overlap with p orbitals localized on the In site. This overlap further explains the phenomenon of interchain coupling observed in $In_2Mo_6Se_6$, as conduction electrons found in a cation orbital are equally likely to subsequently return to any of the three symmetry-equivalent nearest-neighbor $(Mo_6Se_6)_n$ chains.

ACKNOWLEDGMENTS

This work was supported by the Cornell University Materials Science Center and the MRL Program of the National Science Foundation under Award No. DMR-9121654. We would also like to thank Professor Charles P. Slichter and Professor Robert M. Cotts for helpful discussions on multipole expansions.

* Author to whom all correspondence should be addressed.

[1] M. Potel, R. Chevrel, M. Sergent, J. C. Armici, M. Decroux, and O. Fischer, J. Solid State Chem. **35**, 286 (1980).
[2] T. Hughbanks and R. Hoffmann, Inorg. Chem. **21**, 3578 (1982).
[3] J. M. Tarascon, F. J. DiSalvo, and J. V. Waszczak, Solid State Commun. **52**, 227 (1984).
[4] J. M. Tarascon, G. W. Hull, and F. J. DiSalvo, Mater. Res. Bull. **19**, 915 (1984).
[5] M. H. Cohen and F. Reif, in *Solid State Physics: Advances in Research and Applications*, edited by F. Seitz and D. Turnbull (Academic Press, New York, 1957), Vol. 5.
[6] P. C. Taylor, J. F. Baugher, and H. M. Kriz, Chem. Rev. **75**, 203 (1975).
[7] E. N. Kaufmann and R. J. Vianden, Rev. Mod. Phys. **51**, 161 (1979).
[8] G. C. Carter, L. H. Bennett, and D. J. Kahan, *Metallic Shifts in NMR* (Pergamon Press, New York, 1977). (Note that in this book, Rb Knight shifts are referenced to solid RbI, which has a shift of 183 ppm from the more common $1M$ aqueous $RbNO_3$ reference. We have reexpressed the Knight shifts referenced to $RbNO_3$ in the text.)
[9] R. Sternheimer, Phys. Rev. **84**, 244 (1951); **86**, 316 (1952); **95**, 736 (1954).
[10] A. Samoson and E. Lippmaa, J. Magn. Reson. **79**, 255 (1988).
[11] A. P. M. Kentgens, J. J. M. Lemmens, F. M. M. Geurts, and W. S. Veeman, J. Magn. Reson. **71**, 62 (1987).
[12] J. Korringa, Physica **16**, 601 (1950).
[13] K. T. Mueller, J. H. Baltisberger, E. W. Wooten, and A. Pines, J. Phys. Chem. **96** 7001 (1992).
[14] J. H. Baltisberger, S. L. Gann, E. W. Wooten, T. H. Chang, K. T. Mueller, and A. Pines, J. Am. Chem. Soc. **114**, 7489 (1992).
[15] E. Fukushima and S. B. W. Roeder, *Experimental Pulse NMR* (Addison-Wesley, Reading, MA, 1981), p. 109.
[16] G. E. Peterson, C. R. Kurkjian, and A. Carnevale, Phys. Chem. Glasses **15**, 59 (1974).
[17] C. P. Slichter, *Principles of Magnetic Resonance* (Springer-Verlag, New York, 1989), p. 500.
[18] W. W. Simmons and C. P. Slichter, Phys. Rev. **121**, 1580 (1961).
[19] R. A. Bernheim and H. S. Gutowsky, J. Chem. Phys. **32**, 1072 (1960).
[20] G. G. Belford, R. A. Bernheim, and H. S. Gutowsky, J. Chem. Phys. **35**, 1032 (1960).
[21] J. Tegenfeldt and K. Hermansson, Chem. Phys. Lett. **118**, 293 (1985).
[22] B. A. Huggins and P. D. Ellis, J. Am. Chem. Soc. **114**, 2098 (1992).
[23] C. Thibault *et al.*, Nucl. Phys. **A367**, 1 (1981).
[24] C. E. Tanner and C. Wieman, Phys. Rev. A **38**, 1616 (1988).
[25] S. Svanberg and S. Rydberg, Z. Phys. **227**, 216 (1969).
[26] H. Chihara and N. Nakamura, in *Numerical Data and Functional Relationships in Science and Technology*, edited by K.-H. Hellwege and A. M. Hellwege, Landolt-Börnstein, New Series, Group III, Vol. 31, Pt. a (Springer-Verlag, New York, 1993), p. 14.
[27] N. C. Mohapatra, Phys. Rev. A **17**, 829 (1978).
[28] C. Prigge, M. Müller-Warmuth, E. Gocke, and R. Schöllhorn, Chem. Mater. **5**, 1493 (1993).
[29] P. Kusch and T. G. Eck, Phys. Rev. **94**, 1799 (1954).
[30] R. K. Harris and B. E. Mann, *NMR and the Periodic Table* (Academic Press, New York, 1978), p. 287.
[31] T. M. Duncan, *A Compilation of Chemical Shift Anisotropies* (Farragut Press, Chicago, 1990), p. M-7.